Photoacoustics 20 (2020) 100208

Contents lists available at ScienceDirect

Photoacoustics

journal homepage: www.elsevier.com/locate/pacs

A fiber optoacoustic emitter with controlled ultrasound frequency for cell membrane sonoporation at submillimeter spatial resolution

Linli Shi [a], Ying Jiang [b], Yi Zhang [c], Lu Lan [b], Yimin Huang [a], Ji-Xin Cheng [b,d,*], Chen Yang [a,d,*]

[a] Department of Chemistry, Boston University, 580 Commonwealth Avenue, Boston, MA 02215, USA
[b] Department of Biomedical Engineering, Boston University, 44 Cummington Mall, Boston, MA 02215, USA
[c] Department of Physics, Boston University, 590 Commonwealth Avenue, Boston, MA 02215, USA
[d] Department of Electrical and Computer Engineering, 8 St. Mary's Street, Boston, MA 02215, USA

ARTICLE INFO

Keywords:
Optoacoustic
Cell modulation
Sonoporation

ABSTRACT

Focused ultrasound has attracted great attention in minimally invasive therapeutic and mechanism studies. Frequency below 1 MHz is identified preferable for high-efficiency bio-modulation. However, the poor spatial confinement of several millimeters and large device diameter of ~25 mm of typical sub-MHz ultrasound technology suffered from the diffraction limit, severely hindering its further applications. To address it, a fiber-based optoacoustic emitter (FOE) is developed, serving as a miniaturized ultrasound point source, with sub-millimeter confinement, composed of an optical diffusion layer and an expansion layer on an optical fiber. By modifying acoustic damping and light absorption performance, controllable frequencies in the range of 0.083 MHz–5.500 MHz are achieved and further induce cell membrane sonoporation with frequency dependent efficiency. By solving the problem of compromise between sub-MHz frequency and sub-millimeter precision via breaking the diffraction limit, the FOE shows a great potential in region-specific drug delivery, gene transfection and neurostimulation.

1. Introduction

The past decades have seen extensive studies of focused ultrasound for noninvasive or minimally invasive cellular biotechnology, such as drug delivery [1–6], chemogenetics [7], gene transfection [8]– [10], tissue healing delivery [1,11] and neuron stimulation [12,13]. Specifically, focused ultrasound induces transient permeabilization of the cell membrane, i.e. sonoporation, which can facilitate the transport of membrane impermeable compounds into living cells, including low molecular weight drugs, genetic drugs (pDNA, siRNA, mRNA), peptides and proteins [14]. For example, ultrasound assisted drug delivery for treatment of cancers such as pancreatic/lung/breast cancers, showed reduced systemic toxicity through less circulating drug required than traditional chemotherapy [15]. Focused ultrasound mediated gene transfection has also received considerable attention for treating neurological disorders such as Parkinson's disease [16–18]. In previous studies, sub-MHz frequency ultrasound was shown to be more effective [1]. 0.2 MHz ultrasound induces 7 times lower threshold in cavitation compared to high frequency (4.8 MHz) [19]. In the gene transfection study by Huang and coworkers, low frequency 40 kHz ultrasound promoted the transfer of plasmid into bacteria while 850 kHz ultrasound failed [9]. In the neuron stimulation study by Pauly and coworkers, ultrasound of 0.3 MHz showed 150 times lower pressure threshold for successful neuron stimulation compared to 3 MHz [20]. Meanwhile, ultrasound of high frequencies was found to carry higher risk of tissue harmfulness due to its greater heating effects than low frequencies. For example, ultrasound at 1 MHz does not induce cellular alterations while both 2- and 3-MHz frequencies cause complete fat tissue disruption, including destruction of adipose cells and collagenic fibers [21]. Thus, frequency within the range from 20 kHz to 1.0 MHz is considered to be preferable with superior efficiency and reduced heating risk in biomedical applications, including drug delivery, gene transfection and neuron stimulation. However, the typical sub-MHz frequency ultrasound transducers are bulky and poor focusing. A traditional piezo transducer producing ultrasound with a frequency of 1.06 MHz comes with a diameter of 25 mm [22]. Efforts have been made to fabricate miniaturized low frequency transducers, including low-frequency flex tensional resonators, tonpilz transducers, and thickness-type resonators [23]. For example, aiming at ultrasound mediated drug delivery, a piezoelectric disc with an unprecedented thickness of 1 mm and a

* Corresponding authors at: Department of Electrical and Computer Engineering, 8 St. Mary's Street, Boston, MA 02215, USA.
E-mail addresses: jxcheng@bu.edu (J.-X. Cheng), cheyang@bu.edu (C. Yang).

https://doi.org/10.1016/j.pacs.2020.100208
Received 30 March 2020; Received in revised form 9 September 2020; Accepted 10 September 2020
Available online 30 September 2020

diameter of 12.7 mm has been developed to provide acoustic between 1 kHz and 100 kHz depending on the geometry [4]. Nevertheless, fabrication of these transducers with millimeter-scale lateral dimensions is considered challenging and expensive. In addition to its large device size, the transducer-based focus ultrasound technology suffers from large diffraction limited focal volume at millimeter scale for an ultrasound of a few hundred kHz. The ultrasound wave of 1 MHz generated by traditional transducer was found to have a focal width of 4.3 mm [24]. Since the diffraction limit is reversely proportional to the frequency, a desired frequency of 0.2 MHz ultrasound has an even larger focusing diameter, a size comparable to a whole mouse brain (~5.5 × 8 × 14 mm, Allen Brain Atlas database), making it impossible to pinpoint a specific region of the brain using typical transducers. For example, the subthalamic nucleus (STN) is the targeted area of gene transfection for Parkinson's disease [25]. The stimulation of sub-territories of the STN revealed its role in the integration of the emotional and motor aspects of behavior [26]. Thus, the development of ultrasound source providing a sub-millimeter resolution will open up opportunities to target and study the function of specific regional sub-territories area in animal models.

Optoacoustic, in which a pulsed excitation light is absorbed by materials of interest, resulting in transient heating, material compression and expansion, and subsequently pressure change, is a novel way to generate ultrasound. The life sciences have benefitted greatly from optoacoustic tomography technologies [27], in the work of L. V. Wang's group, the optoacoustic tomography can be used in living biological structures ranging from organelles to organs [28]. Meanwhile, fiber-based optoacoustic emission has been explored for miniaturization taking advantage of submillimeter diameters of optical fibers. Thus far, research of fiber-based optoacoustic generation was mainly focused on imaging, targeting an acoustic frequency with a wide bandwidth of tens of MHz. Specifically, in the work from Colchester's group, carbon nanotubes (CNTs) were mixed in polydimethylsiloxane (PDMS), followed by dip coating on an optical fiber tip, which led to a peak frequency at 18 MHz and a bandwidth of 12 MHz [29]. Similarly, Noimark et al. [30] and Poduval et al. [31] coated CNTs and subsequently PDMS on the tip of an optical fiber and showed peak frequency of 20 MHz and 30 MHz, with bandwidth of 23~40 MHz and 29 MHz, respectively. In our previous work, an optical fiber coated with ZnO/Epoxy and Graphite/Epoxy was developed, serving as an optoacoustic guide for sub-millimeter tumor localization and intuitive surgical guidance [32]. To study the involvement of cochlear pathway in the ultrasound induced brain stimulation, the fiber based optoacoustic emitter was used for spatially confined neuron stimulation of mouse brain in vivo [33], showing powerful capability of understanding the bio-interface mechanism. Notably, none of the reported fiber based optoacoustic devices in the literature delivered central sub-MHz frequencies with controllability. Thus, these limitations of current ultrasound and optoacoustic technologies highlight an unmet need of a novel miniaturized ultrasound source together with sub-MHz frequency and a submillimeter spatial precision. Such a device will enable precise and effective cell modulation for targeted therapies, and open up potentials for broader biomedical applications when integrated with other medical devices.

In this work, we report a fiber-based optoacoustic emitter (FOE) with a controllable frequency spectrum, targeting the frequency range of sub-MHz. A key innovation of our device is to design and coat the fiber tip with two distinct functional layers: an optical diffusion layer and a thermal expansion layer, to deliver sufficient ultrasound intensity and to control the peak frequency and bandwidth needed for cell modulation. Employing the FOE that delivers sub-millimeter high special precision ultrasound with 0.083 MHz–5.500 MHz frequency, we investigated the delivery of membrane impermeable small molecules into living cells via sonoporation effect. Delivery was found to be frequency dependent, showing a greater deliver efficiency of Sytox performed under sub-MHz frequency compared to frequency above 1 MHz. Our work offers a new ultrasound point source breaking the acoustic diffraction limitation. By solving the problem of compromise between sub-MHz frequency and sub-millimeter precision, the FOE implicated its broad biomedical applications, including region-specific drug delivery, gene transfection as well as localized neuron stimulation.

2. Results

2.1. Design and fabrication of a two-layer fiber-based optoacoustic emitter

The basic design of the FOE is schematically represented in Fig. 1. To achieve miniaturization, optical fibers were utilized for the laser transmission (Fig. 1b). The FOE is constituted by a light diffusion layer and an absorption/thermal expansion layer (Fig. 1c, d). The diffusion layer was introduced to prevent localized heating and subsequent damage of the expansion layer due to the difference of thermally induced strain within the layer. This diffusion layer comprises a mixture of polymer (Epoxy) and 100-nm diameter zinc oxide (ZnO) nanoparticles, which diffuse the high-energy laser pulse into a Cauchy distribution due to its high optical transparency in the near infrared region and high refractive index [32]. The diameter of ZnO nanoparticles (i.e. 100 nm) is much smaller than the laser wavelength (1030 nm) used, enabling Raleigh scattering in all directions [32]. Then, to convert the light energy into acoustic waves, an absorption/thermal expansion layer was subsequently added as the second coating. It is composed of nanoparticles with high light absorption coefficient as the absorber (multi-wall carbon nanotubes, MWCNTs) and polymer with high thermal expansion coefficient for the purpose of expansion and compression (PDMS). The choosing of materials including MWCNTs and PDMS were done through the comparison with other materials (graphite as absorber, epoxy as expansion matrix) as described in Supplementary materials, aiming at maximizing the optoacoustic conversion efficiency. Taking advantage of these specially designed nano-polymer composite layers at the fiber distal end, upon the pulsed laser excitation, an acoustic wave was effectively generated from the fiber tip through the optoacoustic effect and detected via transducer (Fig. S1). The FOE composed of Epoxy/ZnO as diffusion layer with MWCNTs/PDMS as absorption/thermal expansion layer shows the highest acoustic signal (Fig. S2), indicating a maximized acoustic conversion efficiency. Moreover, to achieve a tunable acoustic pressure, according to the optoacoustic theory, the pressure is proportional to the incident laser fluence. Thus, the amplitude and frequency spectrum of FOE with varied laser fluence is also characterized (Fig. S3), indicating the flexibility of the pressure for different applications.

To realize the controllability of the ultrasound frequency of FOE, the two-layer coating was designed mimicking the structure of a typical transducer. A transducer is composed of three layers [34]: a backing layer to match the specific acoustic impedance between the active layer and the back connector; an active layer (piezo-electric materials to generate ultrasound upon applied voltage) and a matching layer to match the specific acoustic impedance between medium and the active layer (since the specific acoustic impedance of PDMS (1.1–1.5 Pa s/m^3) is close to water (1.48 Pa·s/m^3), the third layer-matching layer can be spared in the FOE). In a transducer, the frequency is determined by two factors. First, the frequency and bandwidth are controlled by the damping effect of the backing layer. Second, the frequency is reversely proportional to the thickness of the active layer [34,35]. In this way, by modifying acoustic damping of the first layer and light absorption thickness of the second layer in the FOE, frequency can be controlled precisely.

2.2. Controlling the ultrasound frequency via modification of the diffusion layer

The first approach of controlling frequency is by modification of the diffusion layer of FOE corresponding to the backing layer of a transducer. The epoxy (specific acoustic impedance: 2.5–3.5 Pa s/m^3) in the

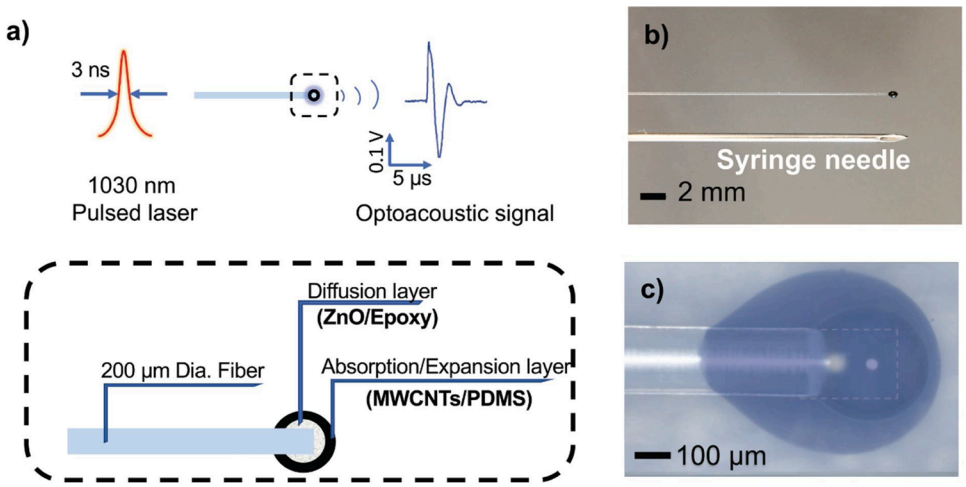

Fig. 1. Design and fabrication of a two-layer fiber-based optoacoustic emitter (FOE). a) Schematic of optoacoustic effect and the design of FOE with a two-layer structure. b) Comparison between the fiber-based emitter and a syringe needle (20 G, ID 0.6 mm, OD 0.91 mm). c) Micrographs of a fabricated FOE. The image transparency was adjusted to visualize the inner diffusion layer and the outer absorption/expansion layer. White dash line outlines the fiber distal end.

diffusion layer acts as the backing layer matrix to match the specific acoustic impedance between the fiber (silica, specific acoustic impedance:13.1 Pa·s/m^3) and the active layer (PDMS, specific acoustic impedance: 1.1–1.5 Pa s/m^3) [36,37]. The damping effect of the backing layer in a typical transducer impacts on the frequency produced, therefore we expect the change of the thickness of the diffusion layer, acting as the backing layer, will control the output frequency of FOE. We fabricated FOEs with ZnO/Epoxy diffusion layer thickness of 36, 42, 53, 62, 79, 100 μm, respectively. Then absorption/thermal expansion layers of CNTs/PDMS with a thickness of 109 ± 24 μm were used. Note that

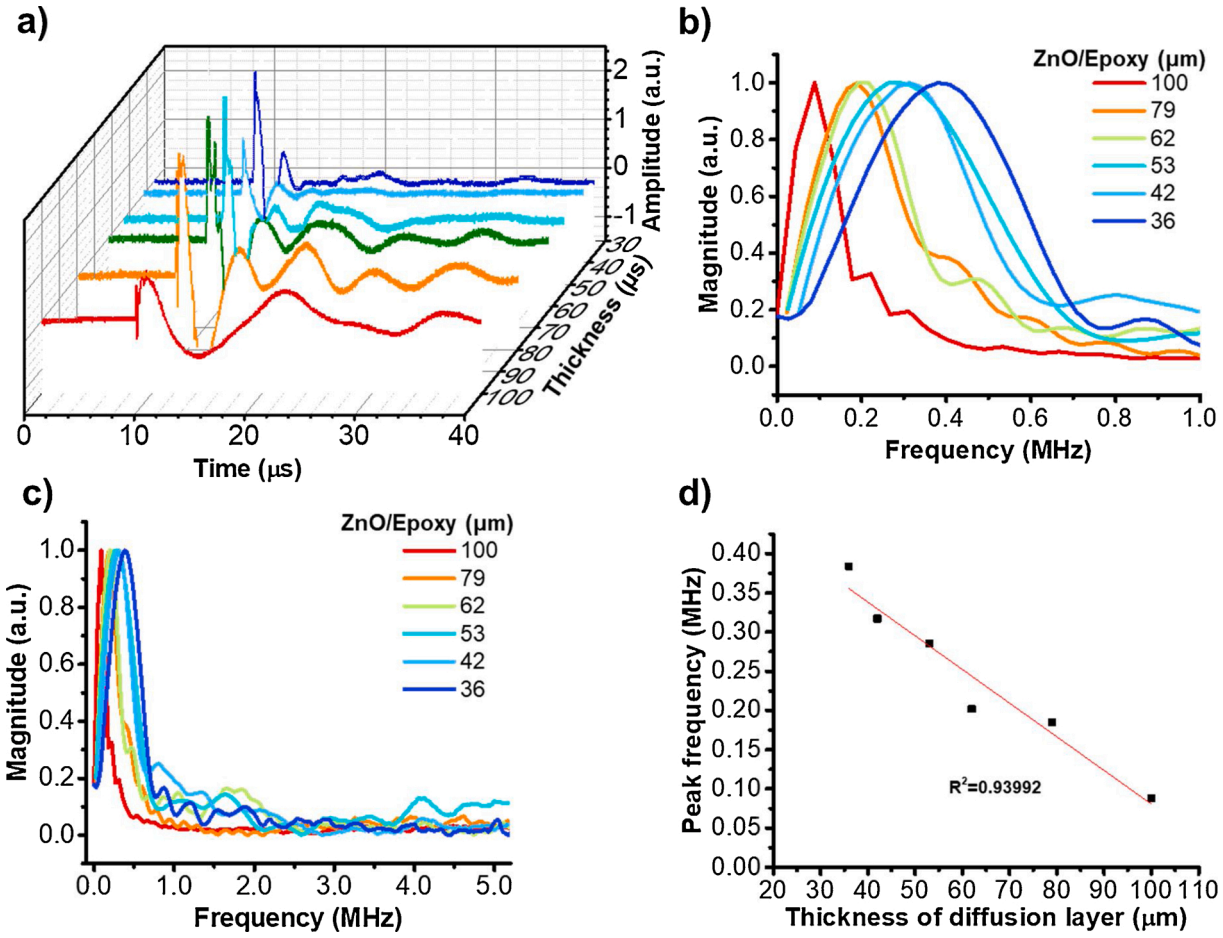

Fig. 2. Controlling the ultrasound frequency via modifying the diffusion layer. a) The ultrasound signals in time domain from FOEs fabricated with diffusion layers (ZnO/Epoxy) of 36−100 μm and absorption/thermal expansion layer (CNTs/PDMS) of 109 ± 24 μm. b) The frequency domain within 0–1.0 MHz of the ultrasound. c) Zoomed-out figure with frequency ranging from 0 to 5.0 MHz. d) Ultrasound peak frequency plotted as a function of the diffusion layer thickness: y = 0.51086-0.00431x, R^2 = 0.93992.

the variation of the thermal expansion layer thickness here doesn't change the ultrasound frequency since they are all beyond the light penetration depth, the theoretical explanation will be in the next section. Then, the time-of-flight optoacoustic signals were recorded (Fig. 2a), processed with FFT and shown in the frequency domain (Fig. 2b). The peak frequency was shown to be controlled in the range of 0.384 to 0.083 MHz through varying the diffusion layer thickness from 36 to 100 μm, suggesting a significant decrease in frequency while increasing the diffusion layer thickness. By examining the frequency range of 0−10 MHz, the distribution of frequencies exhibited a clustering at sub-MHz region (Fig. 2c). In addition, the linear relationship of the frequency and diffusion layer thickness shows an R^2 of 0.93992 with a function of $y = 0.51086\text{-}0.00431x$ (Fig. 2d). Controlling the frequency through changing the diffusion layer can be further rationalized by the fact that the peak frequency of the optoacoustic spectrum could be modulated by the mass of the diffusion layer. The optoacoustic effect can be described by the thermal expansion equation, which is a derivative of the generalized Hooke's law and the equation of motion that is deduced from Newton's second law [38]. During the optoacoustic conversion process, the FOE tip can be regarded as a harmonic oscillator, in which the oscillating motion comes from the initial force given by the thermal expansion effect. In Hooke's law, the amplitude of the oscillation remains constant, and its frequency is independent of its amplitude, but determined by the mass and the stiffness of the oscillator. To this end, the frequency range of 0.083-0.384 MHz is achieved via modifying the Epoxy/ZnO diffusion layer.

Moreover, for typical transducers, the bandwidth is defined by the ratio between the difference of the frequencies at which the spectrum intensity decays to 50 % of its maximum value ($f_{upper} - f_{lower}$) and the central frequency $f_{central}$ [39]:

$$Bandwidth = \frac{f_u - f_l}{f_c} * 100\% \quad (1)$$

The bandwidths for the FOE with central frequencies of 0.083-0.384 MHz were obtained from eq. 1 and shown in Figure S4, showing an average bandwidth of 67.8 ± 6.8 %. These results show that the ultrasound bandwidths generated by FOE were comparable to bandwidths produced by commercial transducers for corresponding frequencies, e.g. 67.09 % for 5 MHz, V326, Olympus; 56.00 % for 10 MHz, XMS310, Olympus. Notably, in commercial transducer, it was found that varying the central frequency via changing the backing layer thickness doesn't change the bandwidth significantly [40], which was coincident with our finding that the FOE bandwidth showed an insignificant frequency dependence (Fig. S4).

2.3. Controlling the ultrasound frequency via altering the CNT concentration in the expansion layer

Another strategy to control the frequency is to change the effective thickness of the active layer (absorption/thermal expansion layer). According to the optoacoustic generation theory, the waveform of optoacoustic is also depending on the light absorption profile of the optoacoustic source, which is $\tau + 1/c\alpha$ (τ is the laser pulse width, α is the light absorption coefficient of the absorber) [41]. The effective thickness of the absorber is determined by the light penetration depth. Therefore, the optoacoustic signal waveform consequentially changes with the effective absorber thickness. We come up with a hypothesis: when the absorber thickness is smaller than the light penetration depth, the frequency is determined by the absorber thickness. When the absorber thickness is larger than the light penetration depth, the frequency will remain constant and the extra thickness only induces acoustic attenuation.

To verify this, first, we investigate how sensitive the change of the peak frequency is to the change of additional physical thickness of expansion layers. Two groups of FOEs were fabricated with ZnO/Epoxy diffusion layers with 36 μm and 100 μm, respectively. For each group, 4 FOEs were made with CNT/PDMS expansion layers varied from 100 μm to 210 μm as indicated by the color legend in Fig. 3, which showed the time domain of ultrasound from FOEs. The waveform remained as similar functions with respect to time while the amplitude was dropping with the increasing of the expansion layer thickness. These are coincident with our hypothesis that when the absorber layer thickness is beyond the light penetration depth, the frequency is not sensitive to the change of the additional physical thickness of expansion layer in the tested range, while the amplitude changing could result from the acoustic attenuation by the extra thickness of the thermal expansion layer.

While the additional physical thickness (beyond light penetration depth) is not a controlling factor for the frequency, we expect to vary the frequency by changing the effective absorber thickness. This can be achieved through modifying the spatial absorption profile of the expansion layer via changing the absorber concentration. Since the effective thickness is primarily determined by the light absorption profile but not the physical thickness, in this way, the influence of fluctuation in the physical thickness and geometric structures would be minimized, improving the robustness of the FOE fabrication. To verify how the absorber concentration can be modified to fine-tune the ultrasound frequency, FOEs were coated only with the CNTs/PDMS expansion layers without the diffusion layers. Different concentrations of CNTs (2.5 %, 5.0 %, 7.5 %, 10.0 % by weight) were used in the mixture. The thickness of the overall coating was kept in the same range. We expect that mixture with lower CNT concentrations allows higher light penetration depths, which subsequently increases the effective thickness, according to the Beer–Lambert law. The results are shown in Fig. 4. From the frequency domain, the FOE with the CNT concentration of 2.5 % generated acoustic waves with a peak frequency of 1.0 MHz compared to the 5.5 MHz from FOE of 10.0 % CNTs concentration. The peak frequency was observed to increase from 1.0 to 5.5 MHz when increasing the concentration. Such CNT concentration dependent frequency change suggests that the controllable peak frequency of optoacoustic can also be achieved by modifying the light absorption profile of the absorption/expansion layer, which is in-line with the acoustic theory discussed above.

Collectively, these two complementary assays (Figs. 3 and 4) demonstrate that, by integrating the frequency control ability of both the diffusion layer and the absorption/thermal expansion layer, we can achieve fine tuning of the frequency within the sub-MHz range as well as frequency beyond 1 MHz.

2.4. Producing consistent frequency in all directions

We further characterized the angular distribution of the acoustic wave in terms of amplitude and frequency spectra. We used a FOE composed of a diffusion layer (ZnO/Epoxy, 40 μm thick) and an expansion layer (CNTs/PDMS, 120 μm thick). The acoustic radiation from the FOE was determined by measuring the output voltage on the oscilloscope at a constant light input of 127 mJ/cm^2. The angle of the transducer detector relative to the fiber axis was varied by a controllable 360° rotation stage (Thorlabs, Inc., NJ, USA) with an accuracy of ±1 °. Optoacoustic signals were acquired at angles of 0°, ±25°, ±50° and ±75°, respectively, as illustrated in Fig. 5a. Fig. 5b and c show the measured acoustic amplitudes. The peak to peak photoacoustic amplitude in Fig. 5c was found to decrease from 5.2 (at 0°) to 1.6 (at ±75°), respectively, which indicated that the larger the angle, the weaker the acoustic amplitude it was, with the maximum amplitude in the front direction. The PA amplitude anisotropy is expected to result from the light intensity anisotropy. Specifically, we have previously measured the angular distribution of light intensity with one layer of ZnO/Epoxy (15 % by weight) [32], angular light intensity distribution was measured using a photodiode mounted on a controllable 360° rotation stage. The light intensity at 50° was approximately 41 % of the light intensity at 0°. In Fig. 5c, the acoustic amplitude at 50° was 37 % of the amplitude at 0°

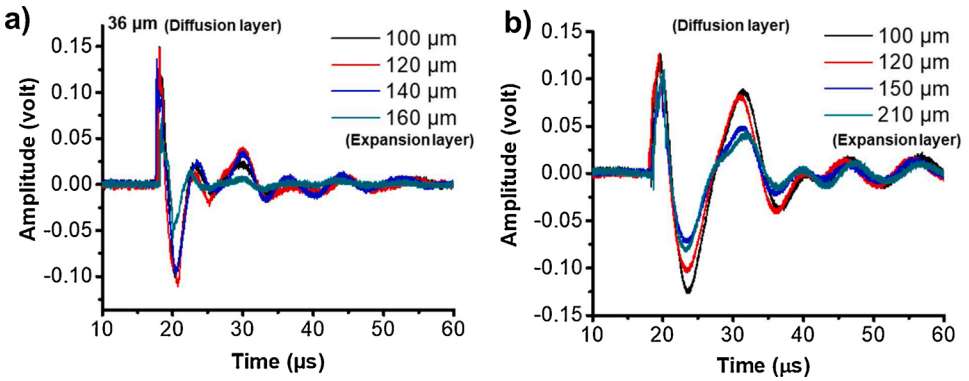

Fig. 3. Characterization the effect of physical thickness of expansion layer on frequency. FOEs with coated with thickness of diffusion layer (36, 100 μm) and with different thickness of absorption/expansion layers as indicated in the color legend. Optoacoustic signals are shown in time domain.

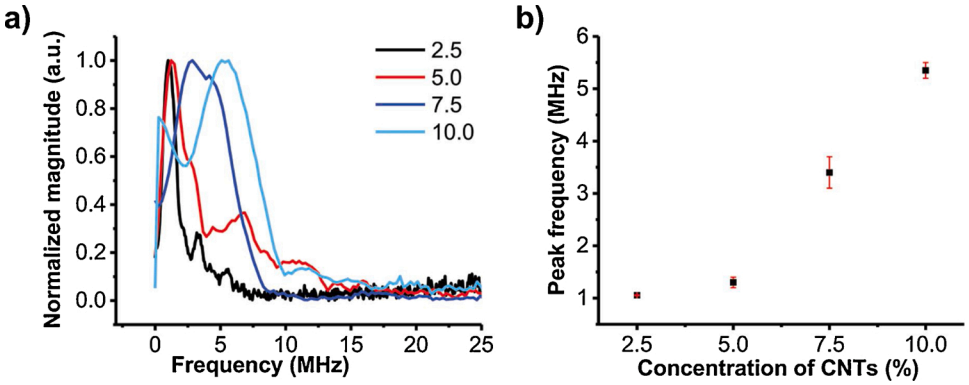

Fig. 4. Optoacoustic signal frequency as a function of effective absorption/expansion layer thickness. a) Normalized frequency spectrum for FOEs with a different thermal expansion layer (CNTs/PDMS, 2.5 %, 5.0 %, 7.5 %, 10.0 % by weight). b) Peak frequency plotted as a function of CNTs/PDMS concentration. Each data point in b) is the average value of two identical FOEs for each concentration and error bars are the standard deviation.

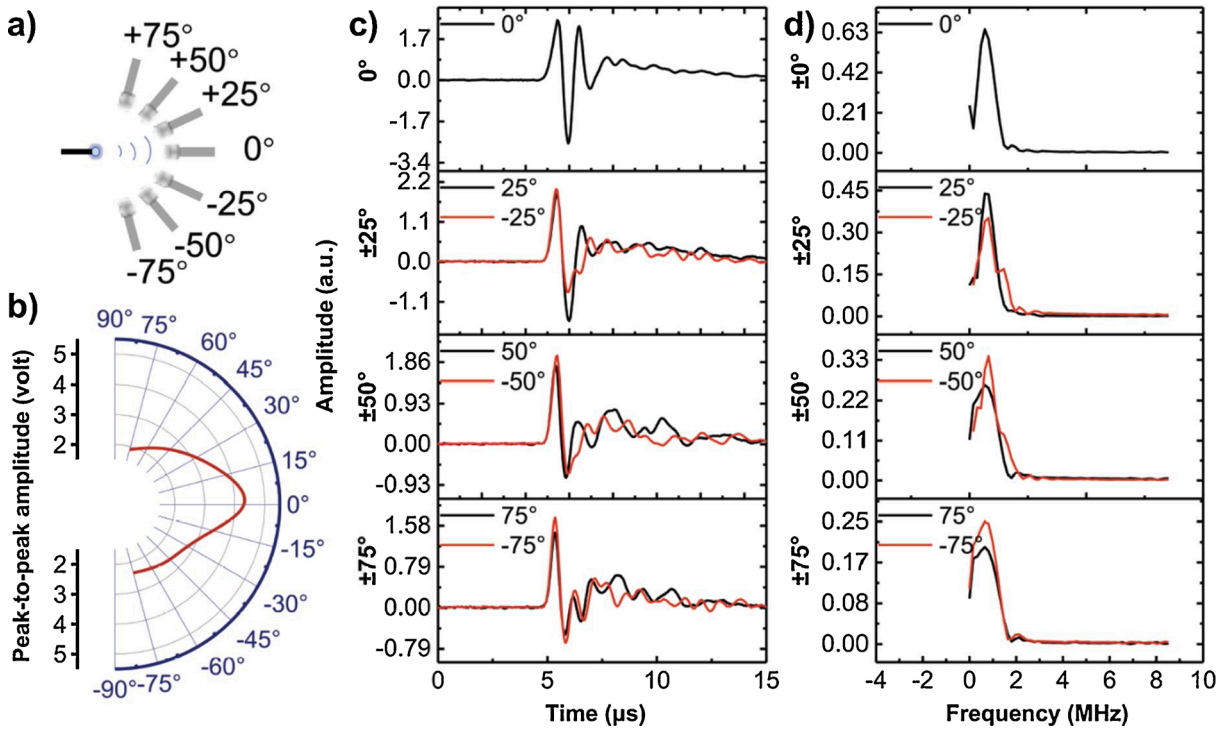

Fig. 5. Characterization of acoustic angular distribution. a) Schematic of the detection. b) Acoustic peak to peak amplitude detected at angles 0°, ±25°, ±50°, and ±75°. c) Angle dependence of acoustic peak-to-peak amplitude. d) Frequency spectra for acoustic signals detected at these angles.

(1.9 V vs. 5.2 V), With the conclusion from Fig. S3, in which the amplitude of photoacoustic signals is proportional to input laser intensity, the acoustic amplitude distribution is consistent with the light intensity distribution data. Fig. 5d shows that the peak frequency was relatively constant (0.7–0.8 MHz) when varying the angle from 0°to ±75°. This is because that majority of the laser pulse energy was delivered along the laser forward direction, despite the effect of diffusion layer, little light propagates laterally, making the lateral optoacoustic induced vibration negligible. Other factors, including the dispersion by the diffusion layer, the curvature radius of the spherical coating, the discrepancy of density and sound speed between PDMS and water, could also contribute to the amplitude anisotropy, which were also worth investigating in the future work. In previous optoacoustic simulation study [42], the optoacoustic wave was conforming to the shape of the fiber tip, which was modeled as a Dirichlet boundary condition on the tip surface. The outer limits of the liquid domain, which was modeled as water, was implemented as plane wave radiation boundary condition. Our finding is consistent with these simulation results, confirming the acoustic wave was scattered and subsequently propagated in all directions, while the acoustic frequency spectrum exhibiting isotropy.

2.5. *The FOE mediated molecule delivery is frequency dependent and shows a spatial confinement of 0.2 mm²*

To demonstrate the superior performance of sub-MHz ultrasound as well as elucidate the spatial confinement of the FOE, cellular uptake of cell membrane impermeable fluorescence molecules during sonoporation mediated by FOEs with varied frequency was evaluated. A high-

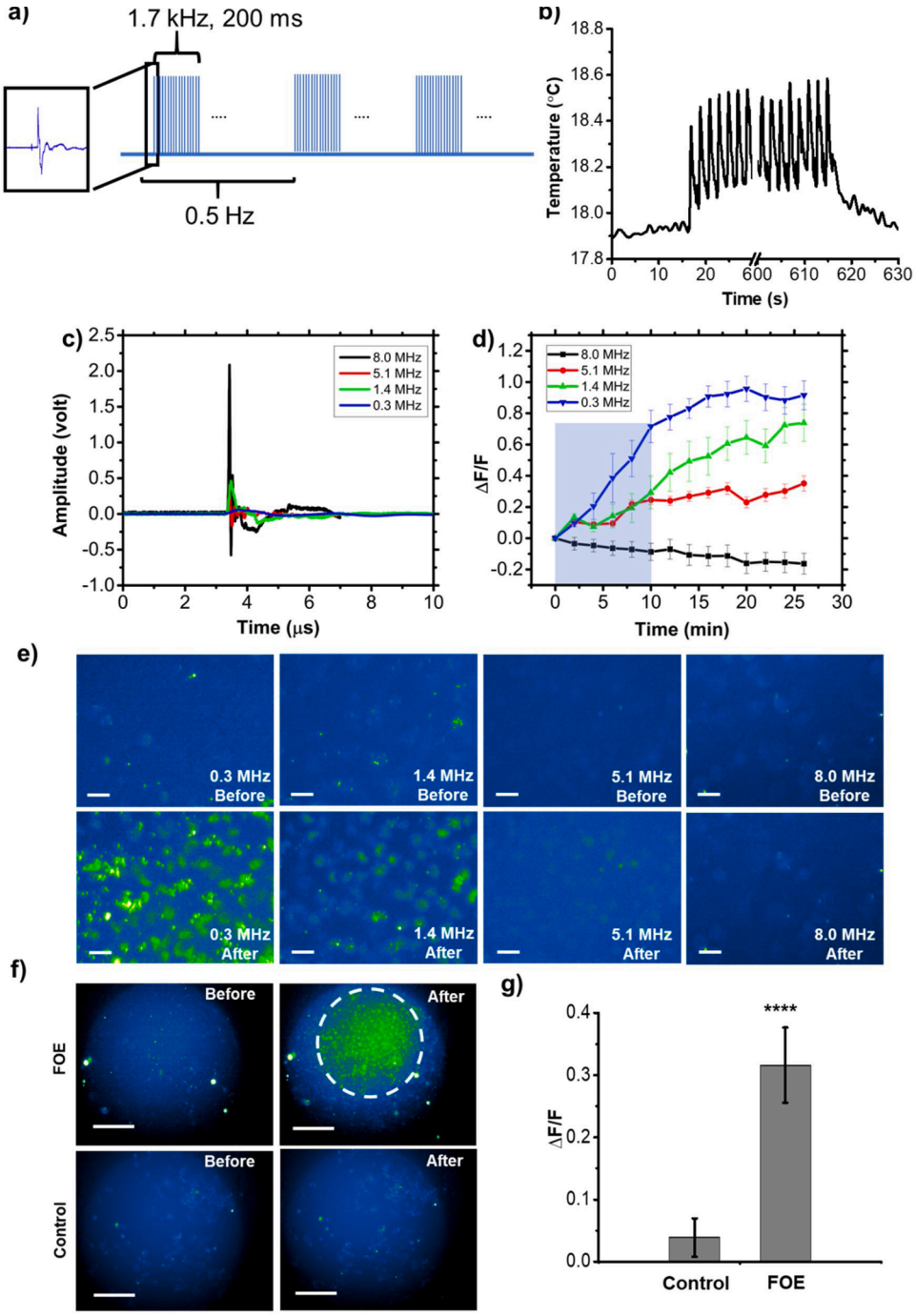

Fig. 6. Frequency dependence of cellular sonoporation induced by FOEs. a) Schematic of laser pulse tone bursts. b) Temperature change at the FOE tip during FOE treatment. Laser is on at 10 s and continued for 8 min. The signal is smoothened without altering the value of temperature change. c) Optoacoustic signals in time domain from FOEs with varied frequency of 8.0, 5.1, 1.4 and 0.3 MHz, respectively. The incident laser fluence was constant at 127 mJ/cm^2. d) Averaged fluorescence intensity changing dynamics of 30 cells upon the treatment of FOEs with varied frequencies for 10 min. e) Fluorescence imaging of FOE treated regions at 0 min (up) and 26 min (down). Scale bar: 50 μm. Blue shadow: laser on for 10 min. f) Fluorescence imaging of FOE treated group and control group taken with 10× objective. The white dash circle indicates the region of significant fluorescence intensity change observed, which was right beneath the position of the FOE at a distance of 100 μm above the cells. g) Comparison of fluorescence intensity change between FOE treated group and control group. **** P<0.0001.

affinity intercalating nucleic acid stain-SYTOX Green, which only penetrates into cells through a compromised plasma membrane and displays fluorescence enhancement upon binding to nucleic acids, was chosen to visualize the sonoporation process. Ultrasound bursts of 200 ms duration were generated using a pulsed laser with 39 mJ/cm^2 at a 1.7 kHz pulse repetition rate, which corresponded to approximately 340 acoustic pulses per burst (Fig. 6a). The optoacoustic treatment was performed at a burst repetition rate of 0.5 Hz in a total period of 10 min. FOEs were placed approximately 100 μm above the cells in culture medium.

First, to exclude the thermal induced cell membrane permeabilization, we measured temperature increase at the fiber tip during the FOE treatment using a miniaturized ultrafast thermal probe (100 μm in diameter) placed in contact with the fiber tip. The temperature rise was found to be 0.6 °C within a total duration of 10 min (Fig. 6b). At such small temperature increase, thermal-induced membrane depolarization is negligible. Therefore, the Sytox uptake results are attributed to mechanical disruption induced by the optoacoustic wave from the FOE.

To study the ultrasound frequency dependence of Sytox uptake efficiency, FOEs with peak frequency of 8.0, 5.1, 1.4 and 0.3 MHz were utilized (8.0 MHz: 15 % CNT/PDMS; 5.1 MHz: 10 % CNT/PDMS; 1.4 MHz: 5 % CNT/PDMS; 0.3 MHz: 15 % ZnO/Epoxy +10 % CNT/PDMS). The ultrasound with varied frequencies was shown in time domain (Fig. 6c). The laser fluence was kept constant to assure identical energy input. The 8.0 MHz signal exhibited the highest amplitude (2.650 V) while the 0.3 MHz signal had the lowest amplitude (0.087 V), which could be partially attributed to the non-uniformity of transducer sensitivity. Fig. 6e shows the fluorescence images of the cell culture before (0 min, upper panels) and after (26 min, lower panels) the FOE treatment. It's clear that when cells are treated with the FOE, cellular uptake of Sytox is significantly increased, indicated by the elevated fluorescence signals. Specifically, 0.3 MHz ultrasound, although with the lowest acoustic intensity, exhibited the highest fluorescence increase after the FOE treatment indicating the highest sonoporation efficiency compared to 1.4 MHz and 5.1 MHz. In comparison, the group treated with 8.0 MHz ultrasound showed negligible Sytox uptake. Overall, the sonoporation efficiency exhibited frequency dependence: the lower the frequency, the higher the cellular uptake efficiency. This conclusion was further demonstrated statistically. In Fig. 6d, the average fluorescence intensity from 30 individual cells treated by varied frequencies were plotted as a function of time. FOE produced 5.1, 1.4 and 0.3 MHz ultrasound all showed increased Sytox fluorescence as a function of time after the treatment, confirming the capability of facilitating Sytox uptake. Fig. 6d also showed a plateau of fluorescence at around 25 min after the treatments indicated that the membrane pores were resealing. The dynamic is consistent with the previous study reported, in which focused ultrasound facilitated the Sytox uptake on the time scale of tens of minutes [43]. Specifically, the curve of the 0.3 MHz group showed the highest slope, meaning that the 0.3 MHz facilitated the Sytox uptake much faster than others. The final reading also demonstrated that 0.3 MHz showed the highest ΔF/F of 0.92 after the FOE treatment indicating the highest sonoporation efficiency compared to 1.4 MHz (ΔF/F = 0.74) and 5.1 MHz (ΔF/F = 0.35). In conclusion, the total amount of uptaken Sytox was frequency dependence: the lower the frequency, the more the molecules pass through the compromised cell membrane within a given period. Furthermore, the 8.0 MHz group did not exhibit significant fluorescence increase but a slight fluorescence decrease. Taking account of the potential influence from photo bleach of Sytox, the reason for overall decline of fluorescence could be that the Sytox uptake induced fluorescence increase was too weak compared to the photo bleach effect. It is conceivable that further increasing the incident laser power to 8.0 MHz ultrasound treatment could eventually result in sonoporation and delivery comparable to the 0.3 MHz group, at the cost of thermal and/or photodamage to the cells. Collectively, the FOE induced sonoporation shows a frequency dependence in which the low frequency performs higher efficiency than high frequency.

To quantify the sonoporation efficiency, we counted the cells with ΔF/F ≥ 50 % as Sytox positive cells and calculated the percentage of Sytox positive cells in the illuminated area. This percentage is taken as a measure of the FOE sonoporation efficiency. For FOEs with frequency of 5.1, 1.4 and 0.3 MHz under the same laser energy and duration, the efficiency obtained from fluorescence imaging at 26 min were found to be 0 %, 72.7 % and 83.3 %, suggesting the lower frequency has substantial higher sonoporation efficiency than the higher frequency ultrasound. Frequency dependence of sonoporation efficiency has been previously reported. Specifically, in the work by Karshafian et al., ultrasound with frequency of 0.5–5.0 MHz was used to deliver 70 kDa FITC-dextran molecules into KHT-C cells, showing permeability increase when decreasing of central frequency [44]. In the work by Miller et al., the pressure threshold of sonoporation of 1.0–3.3 MHz was smaller than the threshold for 5.3 and 7.2 MHz [45]. In Huang's study of ultrasound mediated gene transfection without the assistance of microbubbles, frequency of 40 kHz could efficiently deliver plasmid into bacteria while 850 kHz failed [9]. All these studies agree with our finding that low frequency ultrasound exhibits superior efficiency in sonoporation. The higher efficiency of low frequency ultrasound can be explained by the intramembrane cavitation theory that ultrasound induces bilayer membrane motion, which does not require preexistence of air voids in the tissue. Since the maximum area strain is inversely proportional to the square root of the frequency, the low frequency ultrasound has a lower cavitation threshold, resulting in the improved sonoporation efficacy [46]. In the work of ultrasound induced Sytox uptake with the assistance of microbubbles [47], the maximum percentages of MDA-MB-468 cells with uptake were less than 20 % following sonication for 15 ms (150 cycles with pulse duration of 100 μs) with 400, 500 and 600 kPa, respectively (threshold of ΔF/F unknown). In our work, FOE provides pressure around 40 kPa with effective sonication duration of 1.1 ms (340 pulses, pulse duration less than 3.3 μs), and enables sonoporation efficiency of 72.7 % and 83.3 % for low frequency. Thus, the low frequency localized optoacoustic wave generated by FOE shows comparable performance although the test cells are different.

To validate that the FOE provides a unique strategy to enable localized regional cell modulation through the localized delivery of specific molecules to cells by the confinement of the sonoporation, compared to typical the whole cell dish modulation, fluorescence increase of cell cultures were examined with a 10× field. The localized delivery was shown in Fig. 6f and g. After the FOE treatment, the treated region with an area of 0.2 mm^2 exhibited significant fluorescence increase of 32 %, indicating a spatial confinement of 0.2 mm^2 laterally. To further validate the localization, since the conventional transducer array is diffraction limited in the sub-MHz range, the FOE induced cell modulation in tissue using two-photon imaging would reveal the spatial confinement via 3-dimentional visualization. Next, to test the bio-safety of FOE, using 2 μg/mL Propidium Iodide staining (Thermo Fisher Scientific, Waltham, MA, USA), the cell viability after FOE treatment was found to be 99.55 ± 0.03 % (Fig. S5), indicating the superior biocompatibility of FOE treatment. Collectively, the FOE used as a novel ultrasound source for small molecule delivery into cells exhibited frequency dependence, indicating the significance of sub-MHz ultrasound. The localized fluorescence change is indicative of the 0.2 mm^2 spatial confinement of the FOE, holding promise for cell modulation with high spatial precision, including neuron stimulation as well as localized gene transfection for gene-protein studies.

3. Conclusion

Fiber based photoacoustic emitters composed of nanoparticle-polymer matrix with superior optical and mechanical properties were designed and fabricated. The two-layer coating design, including a diffusion layer and an expansion layer, provides precise controllability in amplitude and frequency of the ultrasound generated. Localized acoustic wave generation with high amplitude and tunable frequency in the sub-MHz range were achieved. By characterizing the optoacoustic

signal profile in amplitude and frequency spectrum, a matrix of CNTs/PDMS was demonstrated to be a preferable candidate to achieve high amplitudes. Two effective strategies to control the acoustic frequency were demonstrated. First, the frequency was varied by the thickness of the diffusion layer, which acted as damping material via the acoustic impedance mismatch. Second, the acoustic frequency is also controlled by the depth of light penetration through the active absorber/expansion layer, which has been indirectly controlled by changing the absorber concentration. By using the FOEs with varied frequency ranging from 0.3 MHz to 8.0 MHz for small molecules delivery into cell membrane, sub-MHz ultrasound exhibited superior efficiency compared to high frequency. A lateral spatial confinement of 0.2 mm^2 was also confirmed by the sonoporation effective area. Thus, a sub-MHz frequency acoustic with sub-millimeter confinement was produced using the miniaturized FOE, overcoming the limitation of other typical ultrasound sources. Such FOE device design holds promise for a wide range of cellular applications, including cell membrane sonoporation, and offers new tools for localized drug delivery, neuron stimulation and gene transfection with high efficacy and minimized safety issue.

By achieving the high miniaturization levels demonstrated, the tunable optoacoustic emitters are promising for minimally invasive medical applications, where the fiber based optoacoustic devices presented here could be inserted in syringe needles or catheters in close proximity to a focal lesion, thus overcoming the problem of reduced precision and amplitude induced by traditional focused ultrasound. Further experiment can be carried out to improve the performance. For example, the laser beam can be coupled to the fiber using higher order modes for optimum optoacoustic signal generation. Second, the shape of FOE tip might provide opportunity to focus the wave via concave structure. Third, further validating the localization of the sub-millimeter is challenging, since the conventional transducer array is diffraction limited in the sub-MHz range. The FOE induced cell modulation in tissue using two-photon imaging would reveal the spatial confinement via 3-dimentional visualization. Under a broader context, this technique offers the potential to generate stable and reversible sonoporation at each focal target through modification of the ultrasound parameters, enabling precise control for biomedical ultrasound application, which is not available with existing technologies, especially for drug delivery and gene transfer. Additionally, this FOE is immune to electromagnetic interference and hence is compatible with magnetic resonance imaging (MRI) [48]. These flexibilities, along with its unprecedentedly miniaturization, and amenability to be readily repeated, make it a potentially transformative technology.

4. Experimental section

4.1. Fabrication of a two-layer fiber-based optoacoustic emitter (FOE)

The fabrication of FOE is composed of two steps. First, for the diffusion layer, the Epoxy or PDMS matrix was prepared via cross linking process. Epoxy was made by mixing polyepoxides solution (Devcon Inc, Alberta, Canada) with polyfunctional curatives in a ratio of 1:1 by volume. For PDMS, the silicone elastomer (*Sylgard* 184, Dow Corning Corporation, USA) was dispensed directly into the container carefully to minimize air entrapment, followed by mixing with the curing agent in a ratio of 10:1 by weight. Subsequently, ZnO nanoparticles serving as diffuser (~100 nm, Sigma-Aldrich, Inc., MO, USA) were added into the matrix at a concentration of 15 % by weight otherwise specified. The concentration was chosen based on previous optimization study to achieve a uniform distributed laser emission [32]. A multimode optical fiber with 200 μm core diameter (FT200EMT, Thorlabs, Inc., NJ, USA) and a polished distal end was carefully dipped about 100 μm below the surface of the mixture solution and then quickly pulled up, using a micro manipulator. By placing vertically at room temperature, the polymer crosslinked and the matrix formed the coating. The diffusion layer made of Epoxy was subsequently coated with the absorption/thermal expansion layer of Epoxy. In this way, the specific acoustic impedance mismatch was minimized, providing the maximized optoacoustic conversion efficiency. Graphite powder (Dick Blick Holdings, Inc., IL, USA) was mixed with the matrix at a concentration of 30 % by weight. MWCNTs, (<8 nm OD, 2−5 nm ID, Length 0.5−2 μm, VWR, Inc., NY, USA) was used at a concentration of 0–10 % by weight, approaching the solubility upper limit owing to its low density (1.65 g/cm^2). Similarly, the FOEs made of PDMS matrix were fabricated. In the latter experiment of FOE generating the sub-MHz frequencies, the structure was modified as ZnO/Epoxy (the diffusion layer) and CNTs/PDMS (the absorption/thermal expansion layer), in which Epoxy and PDMS realized specific acoustic impedance mismatch. In this way, the pressure was compromised while still meeting the frequency need for cell modulation. By making a mark near the fiber tip with thermal resist ink, the thickness after coating was measured by aligning the mark on the before-and-after micrograph.

Light leak would generate acoustic response on the detecting transducer due to the pulsed laser induced shockwave in water and transducer probe [49], and potentially cause damage of the detector. A power meter was used to measure light transmittance to evaluate the light leak. We found the design and fabrication discussed above eliminated the light leak of FOEs. For all FOEs with different materials and geometric structure throughout the study, a light transmittance of less than 0.5 % was ensured by multiple coating of absorption/thermal expansion layer.

4.2. Ultrasound generation and characterization

A thorough acoustic characterization of the generated optoacoustic waves was carried out by a setup shown in Fig. S1. A Q-Switched laser (Bright Solutions, Inc., AK, USA) with a wavelength of 1030 nm and a pulse width of 3 ns was used as the laser source. The laser fluence was 127 mJ/cm^2 unless otherwise specified. Two functional generators were used to give laser pulses in a tone burst mode. Functional generator 1 provided triggers with repetition rate of 0.5 Hz as the tone burst frequency. For each burst, the functional generator 2 provided triggers with repetition rate of 1.7 kHz and burst duration of 0.2 s. In the measurement setup, an ultrasound transducer (5 MHz, V326, Olympus, MA) together with an ultrasonic pre-amplifier (0.2–40 MHz, 40 dB gain, Model 5678, Olympus, USA) was utilized to characterize the frequency of the ultrasonic waves. To quantify the acoustic pressure, a needle hydrophone with a diameter of 40 μm and frequency range of 1−20 MHz (NH0040, Precision Acoustics Inc., Dorchester, UK) was utilized together with the pre-amplifier. The distance between the FOE tips and transducer was kept at 1.50 mm and at 0.1 mm between the FOE tips and hydrophone. A digital oscilloscope (DSO6014A, Agilent Technologies, CA) was used to display the readout electrical signal from the transducer or hydrophone. The FOE and transducer/hydrophone were all immersed in deionized water to mimic the typical environment related to biomedical application and to minimize the specific acoustic impedance mismatch among the FOE, water and detectors.

4.3. Cell culture and fluorescence microscopy

For the sonoporation experiments, MIA PaCa-2 (Human Caucasian pancreatic carcinoma cell, American Tissue Cell Culture Manassas, VA, USA) were seeded in 35 mm glass bottom dishes with a cell density of 8×10^4/ml and a confirmed viability of 80–95 % prior to the ultrasound treatment. Sytox Green Nucleic Acid Stain (Thermo Fisher Scientific, Waltham, MA, USA) in phosphate buffer solution (PBS) was added to the cell culture dish to reach a final concentration of 10 μM immediately followed by the ultrasound treatment with conditions described later. To minimize the influence of laser induced cytotoxicity, time-lapse fluorescence images were taken every 2 min using an inverted wide-field fluorescence microscope with a LED at 470 nm as excitation light source. Images were acquired by a scientific CMOS camera (Zyla 5.5, Andor).

Declaration of Competing Interest

The authors declare that they have no known competing financial interests or personal relationships that could have appeared to influence the work reported in this paper.

Acknowledgment

This research was supported by R01 NS109794 to J-XC and Boston University Nanotechnology Innovation Center Pilot Grant (2018-2019) to CY. LS, LL, CY and J-XC conceived this project. LS, YZ and LL designed the FOE system, LS and YZ built the characterization set up. LS and YH performed the experiments. LS, YJ and YH implemented the sonoporation experiment. LS, J-XC and CY wrote the manuscript. CY and J-XC provided overall guidance for the project. The authors declare that all of the data supporting the findings of this study are available within the paper and the supplementary information.

Appendix A. Supplementary data

Supplementary material related to this article can be found, in the online version, at doi:https://doi.org/10.1016/j.pacs.2020.100208.

References

[1] S. Mitragotri, Healing sound: the use of ultrasound in drug delivery and other therapeutic applications, Nat. Rev. Drug Discov. 4 (3) (2005) 255–260.
[2] K.W. Ferrara, Driving delivery vehicles with ultrasound, Adv. Drug Deliv. Rev. 60 (10) (2008) 1097–1102.
[3] N.B. Smith, S. Lee, E. Maione, R.B. Roy, S. McElligott, K.K. Shung, Ultrasound-mediated transdermal transport of insulin in vitro through human skin using novel transducer designs, Ultrasound Med. Biol. 29 (2) (2003) 311–317.
[4] E. Park, J. Werner, N.B. Smith, Ultrasound mediated transdermal insulin delivery in pigs using a lightweight transducer, Pharm. Res. 24 (7) (2007) 1396–1401.
[5] T. Sun, Y. Zhang, C. Power, P.M. Alexander, J.T. Sutton, M. Aryal, N. Vykhodtseva, E.L. Miller, N.J. McDannold, Closed-loop control of targeted ultrasound drug delivery across the blood–brain/tumor barriers in a rat glioma model, Proc. Natl. Acad. Sci. 114 (48) (2017) E10281–E10290.
[6] M. Kinoshita, N. McDannold, F.A. Jolesz, K. Hynynen, Noninvasive localized delivery of Herceptin to the mouse brain by MRI-guided focused ultrasound-induced blood–brain barrier disruption, Proc. Natl. Acad. Sci. 103 (31) (2006) 11719–11723.
[7] J.O. Szablowski, A. Lee-Gosselin, B. Lue, D. Malounda, M.G. Shapiro, Acoustically targeted chemogenetics for the non-invasive control of neural circuits, Nat. Biomed. Eng. 2 (7) (2018) 475.
[8] H. Liang, J. Tang, M. Halliwell, Sonoporation, drug delivery, and gene therapy, Proc. Inst. Mech. Eng. H 224 (2) (2010) 343–361.
[9] Y. Song, T. Hahn, I.P. Thompson, T.J. Mason, G.M. Preston, G. Li, L. Paniwnyk, W. E. Huang, Ultrasound-mediated DNA transfer for bacteria, Nucleic Acids Res. 35 (19) (2007) e129.
[10] M. Shimamura, N. Sato, Y. Taniyama, S. Yamamoto, M. Endoh, H. Kurinami, M. Aoki, T. Ogihara, Y. Kaneda, R. Morishita, Development of efficient plasmid DNA transfer into adult rat central nervous system using microbubble-enhanced ultrasound, Gene Ther. 11 (20) (2004) 1532–1539.
[11] T.M. Best, K.E. Wilk, C.T. Moorman, D.O. Draper, Low intensity ultrasound for promoting soft tissue healing: a systematic review of the literature and medical technology, Internal Med. Rev. (Washington, DC: Online) 2 (11) (2016).
[12] D. Folloni, L. Verhagen, R.B. Mars, E. Fouragnan, C. Constans, J.-F. Aubry, M. F. Rushworth, J. Sallet, Manipulation of subcortical and deep cortical activity in the primate brain using transcranial focused ultrasound stimulation, Neuron 101 (6) (2019) 1109–1116, e5.
[13] W.J. Tyler, S.W. Lani, G.M. Hwang, Ultrasonic modulation of neural circuit activity, Curr. Opin. Neurobiol. 50 (2018) 222–231.
[14] I. Lentacker, I. De Cock, R. Deckers, S. De Smedt, C. Moonen, Understanding ultrasound induced sonoporation: definitions and underlying mechanisms, Adv. Drug Deliv. Rev. 72 (2014) 49–64.
[15] J. Qin, T.-Y. Wang, J.K. Willmann, Sonoporation: applications for cancer therapy. Therapeutic Ultrasound, Springer, 2016, pp. 263–291.
[16] C.-H. Fan, C.-Y. Ting, C.Y. Lin, H.-L. Chan, Y.-C. Chang, Y.-Y. Chen, H.-L. Liu, C.-K. Yeh, Noninvasive, targeted, and non-viral ultrasound-mediated GDNF-plasmid delivery for treatment of Parkinson's disease, Sci. Rep. 6 (2016) 19579.
[17] L. Long, X. Cai, R. Guo, P. Wang, L. Wu, T. Yin, S. Liao, Z. Lu, Treatment of Parkinson's disease in rats by Nrf2 transfection using MRI-guided focused ultrasound delivery of nanomicrobubbles, Biochem. Biophys. Res. Commun. 482 (1) (2017) 75–80.
[18] G. Leinenga, C. Langton, R. Nisbet, J. Götz, Ultrasound treatment of neurological diseases—current and emerging applications, Nat. Rev. Neurol. 12 (3) (2016) 161.
[19] T.T. Nguyen, Y. Asakura, S. Koda, K. Yasuda, Dependence of cavitation, chemical effect, and mechanical effect thresholds on ultrasonic frequency, Ultrason. Sonochem. 39 (2017) 301–306.
[20] P.P. Ye, J.R. Brown, K.B. Pauly, Frequency dependence of ultrasound neurostimulation in the mouse brain, Ultrasound Med. Biol. 42 (7) (2016) 1512–1530.
[21] G.A. Ferraro, F. De Francesco, G. Nicoletti, F. Rossano, F. D'Andrea, Histologic effects of external ultrasound-assisted lipectomy on adipose tissue, Aesthetic Plast. Surg. 32 (1) (2008) 111–115.
[22] R.S. Mulik, C. Bing, M. Ladouceur-Wodzak, I. Munaweera, R. Chopra, I.R. Corbin, Localized delivery of low-density lipoprotein docosahexaenoic acid nanoparticles to the rat brain using focused ultrasound, Biomaterials 83 (2016) 257–268.
[23] N.B. Smith, Perspectives on transdermal ultrasound mediated drug delivery, Int. J. Nanomed. 2 (4) (2007) 585.
[24] G.-F. Li, H.-X. Zhao, H. Zhou, F. Yan, J.-Y. Wang, C.-X. Xu, C.-Z. Wang, L.-L. Niu, L. Meng, S. Wu, Improved anatomical specificity of non-invasive neuro-stimulation by high frequency (5 MHz) ultrasound, Sci. Rep. 6 (2016) 24738.
[25] P.A. LeWitt, A.R. Rezai, M.A. Leehey, S.G. Ojemann, A.W. Flaherty, E.N. Eskandar, S.K. Kostyk, K. Thomas, A. Sarkar, M.S. Siddiqui, AAV2-GAD gene therapy for advanced Parkinson's disease: a double-blind, sham-surgery controlled, randomised trial, Lancet Neurol. 10 (4) (2011) 309–319.
[26] L. Mallet, M. Schüpbach, K. N'Diaye, P. Remy, E. Bardinet, V. Czernecki, M.-L. Welter, A. Pelissolo, M. Ruberg, Y. Agid, Stimulation of subterritories of the subthalamic nucleus reveals its role in the integration of the emotional and motor aspects of behavior, Proc. Natl. Acad. Sci. 104 (25) (2007) 10661–10666.
[27] L.V. Wang, J. Yao, A practical guide to photoacoustic tomography in the life sciences, Nat. Methods 13 (8) (2016) 627.
[28] L.V. Wang, S. Hu, Photoacoustic tomography: in vivo imaging from organelles to organs, Science 335 (6075) (2012) 1458–1462.
[29] R.J. Colchester, C.A. Mosse, D.S. Bhachu, J.C. Bear, C.J. Carmalt, I.P. Parkin, B. E. Treeby, I. Papakonstantinou, A.E. Desjardins, Laser-generated ultrasound with optical fibres using functionalised carbon nanotube composite coatings, Appl. Phys. Lett. 104 (17) (2014), 173502.
[30] S. Noimark, R.J. Colchester, B.J. Blackburn, E.Z. Zhang, E.J. Alles, S. Ourselin, P. C. Beard, I. Papakonstantinou, I.P. Parkin, A.E. Desjardins, Carbon-nanotube–PDMS composite coatings on optical fibers for all-optical ultrasound imaging, Adv. Funct. Mater. 26 (46) (2016) 8390–8396.
[31] R.K. Poduval, S. Noimark, R.J. Colchester, T.J. Macdonald, I.P. Parkin, A. E. Desjardins, I. Papakonstantinou, Optical fiber ultrasound transmitter with electrospun carbon nanotube-polymer composite, Appl. Phys. Lett. 110 (22) (2017), 223701.
[32] L. Lan, Y. Xia, R. Li, K. Liu, J. Mai, J.A. Medley, S. Obeng-Gyasi, L.K. Han, P. Wang, J.-X. Cheng, A fiber optoacoustic guide with augmented reality for precision breast-conserving surgery, Light Sci. Appl. 7 (1) (2018) 2.
[33] Y. Jiang, H.J. Lee, L. Lan, H.-a. Tseng, C. Yang, H.-Y. Man, X. Han, J.-X. Cheng, Optoacoustic brain stimulation at submillimeter spatial precision, Nat. Commun. 11 (1) (2020) 1–9.
[34] M. Lethiecq, F. Levassort, D. Certon, L.P. Tran-Huu-Hue, Piezoelectric transducer design for medical diagnosis and NDE. Piezoelectric and Acoustic Materials for Transducer Applications, Springer, 2008, pp. 191–215.
[35] C.S. Desilets, J.D. Fraser, G.S. Kino, The design of efficient broad-band piezoelectric transducers, IEEE Trans. Sonics Ultrason. 25 (3) (1978) 115–125.
[36] R.-M. Guillermic, M. Lanoy, A. Strybulevych, J.H. Page, A PDMS-based broadband acoustic impedance matched material for underwater applications, Ultrasonics 94 (2019) 152–157.
[37] https://www.nde-ed.org/GeneralResources/MaterialProperties/UT/ut_matlprop_ceramics.htm.
[38] E. Svanström, Analytical photoacoustic model of laser-induced ultrasound in a planar layered structure, Luleå tekniska universitet (2013).
[39] V.M. do Nascimento, V.L.d.S.N. Button, J.M. Maia, E.T. Costa, E.J.V. Oliveira, Influence of backing and matching layers in ultrasound transducer performance, Medical Imaging 2003: Ultrasonic Imaging and Signal Processing, International Society for Optics and Photonics (2003) 6–96.
[40] K. Nicolaides, L. Nortman, J. Tapson, The effect of backing material on the transmitting response level and bandwidth of a wideband underwater transmitting transducer using 1-3 piezocomposite material, Phys. Procedia 3 (1) (2010) 1041–1045.
[41] T. Lee, H.W. Baac, Q. Li, L.J. Guo, Efficient photoacoustic conversion in optical nanomaterials and composites, Adv. Opt. Mater. 6 (24) (2018), 1800491.
[42] M. Mohammadzadeh, S.R. Gonzalez-Avila, Y.C. Wan, X. Wang, H. Zheng, C.-D. Ohl, Photoacoustic shock wave emission and cavitation from structured optical fiber tips, Appl. Phys. Lett. 108 (2) (2016), 024101.
[43] B. Lammertink, R. Deckers, M. Derieppe, I. De Cock, I. Lentacker, G. Storm, C. T. Moonen, C. Bos, Dynamic fluorescence microscopy of cellular uptake of intercalating model drugs by ultrasound-activated microbubbles, Mol. Imaging Biol. 19 (5) (2017) 683–693.
[44] R. Karshafian, P.D. Bevan, R. Williams, S. Samac, P.N. Burns, Sonoporation by ultrasound-activated microbubble contrast agents: effect of acoustic exposure parameters on cell membrane permeability and cell viability, Ultrasound Med. Biol. 35 (5) (2009) 847–860.
[45] D.L. Miller, S. Bao, J.E. Morris, Sonoporation of cultured cells in the rotating tube exposure system, Ultrasound Med. Biol. 25 (1) (1999) 143–149.
[46] B. Krasovitski, V. Frenkel, S. Shoham, E. Kimmel, Intramembrane cavitation as a unifying mechanism for ultrasound-induced bioeffects, Proc. Natl. Acad. Sci. 108 (8) (2011) 3258–3263.

[47] B. Lammertink, R. Deckers, G. Storm, C. Moonen, C. Bos, Duration of ultrasound-mediated enhanced plasma membrane permeability, Int. J. Pharm. 482 (1–2) (2015) 92–98.
[48] S. Noimark, R.J. Colchester, R.K. Poduval, E. Maneas, E.J. Alles, T. Zhao, E. Z. Zhang, M. Ashworth, E. Tsolaki, A.H. Chester, Polydimethylsiloxane composites for optical ultrasound generation and multimodality imaging, Adv. Funct. Mater. 28 (9) (2018), 1704919.
[49] B. Fairand, A. Clauer, Laser generation of high-amplitude stress waves in materials, J. Appl. Phys. 50 (3) (1979) 1497–1502.

Linli Shi received her B.Sc and M.Sc degree from Sichuan University. She is currently working in Boston University focusing on material interface for biomedical applications including cell modulation and neuron stimulation.

Ying Jiang received the B.Sc degree in biomedical engineering from Shanghai Jiaotong University. He is currently a graduate research assistant in Boston University. His research interests include neuron stimulation using ultrasonic and photoacoustic waves.

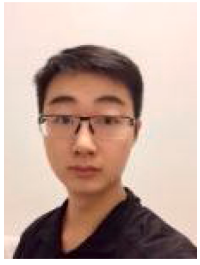

Yi Zhang received the B.Sc degree in 2015 from University of Science and Technology of China. He is currently working on Mid-infrared photothermal microscopy.

Lu Lan received the B.Sc degree in Optical Engineering from South China University of Technology, M.Sc degree from Zhejiang University, and recently received the Ph.D. degree in Biomedical Engineering from Boston University. His research interests include biomedical imaging and sensing, and clinical translation.

Yimin Huang received the B.Sc/ M.Sc degree in Materials Physics and Chemistry from University of Science and Technology of China. Her research interests include nano-bio interfaces for cell modulation.

Ji-xin Cheng received the B.Sc degree and Ph.D. degree from the University of Science and Technology of China (USTC). As a graduate student, he worked as a research assistant at Universite Paris-sud and the Hong Kong University of Science and Technology (HKUST). After the first postdoc training with Professor Yijing Yan at HKUST, Cheng joined Professor Sunney Xie's group at Harvard University as a postdoctoral fellow in 2000. In 2003, Cheng moved to Purdue University as an assistant professor in the Weldon School of Biomedical Engineering and Department of Chemistry. Cheng joined Boston University since 2017 as Moustakas Chair Professor in Photonics and Optoelectronics. Cheng has been building a multidisciplinary and collaborative research program that spans the areas of membrane and cell biophysics, biomedical imaging, and development of new microscopy tools.

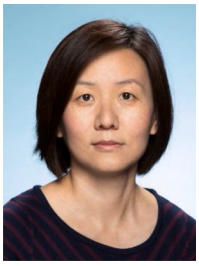

Chen Yang received the bachelor degree in Chemical Physics from University of Science and Technology of China in 1999, the Master of Philosophy from Hong Kong University of Science and Technology in 2000, and the doctoral degree in Chemistry from Harvard University in 2006. She was an associate in McKinsey & Co in 2006 and 2007. She joined Department of Chemistry and Department of Physics as an Assistant Professor at Purdue University in August 2007. Dr. Yang is currently an Associate Professor in Department of Electrical and Computer Engineering and Department of Chemistry at Boston University.